

# Phase diagram and optical conductivity of the ionic Hubbard model

Ph. Brune <sup>a</sup>, G. I. Japaridze <sup>a,b</sup>, A. P. Kampf <sup>a</sup>, and M. Sekania <sup>a</sup>

<sup>a</sup> *Institut für Physik, Theoretische Physik III, Elektronische Korrelationen und Magnetismus, Universität Augsburg, 86135 Augsburg, Germany*

<sup>b</sup> *Institute of Physics, Georgian Academy of Sciences, Guramishvili Str. 6, 380077, Tbilisi, Georgia*

We investigate the ground-state phase diagram of the one-dimensional “ionic” Hubbard model with an alternating periodic potential at half-filling by the bosonization technique as well as by numerical diagonalization of finite systems with the Lanczos and density matrix renormalization group (DMRG) methods. Our results support the existence of a single “metallic” transition point from a band to a correlated insulator with simultaneous charge and bond-charge order. In addition, we present results for the optical conductivity obtained by the dynamical DMRG method. The insulator-insulator phase transition scenario is discussed in detail including a critical review of existing approaches and results for the ionic Hubbard model.

PACS numbers: 71.10.-w, 71.10.Fd, 71.10.Hf, 71.27.+a, 71.30.+h

## I. INTRODUCTION

For more than two decades the correlation induced metal-insulator transition (MIT) and its characteristics has been one of the challenging problems in condensed matter physics [1]. This MIT is often accompanied by a symmetry breaking and the development of long range order [2]. In dimension  $D=1$  this ordering can only be connected with the breaking of a discrete symmetry. Examples include commensurate charge density waves (CDWs) and Peierls dimerization phenomena. The MIT can be driven either by varying the electron density or the electron-electron interaction strength. If the MIT is approached from the metallic side, the electrical conductivity or the electronic compressibility may be used to characterize the transition; the approach of the transition from the insulating side may on the other hand be properly captured by the divergent behavior of the electric susceptibility [3].

In addition, the features of the insulating phase may change qualitatively with the interaction strength, allowing for quantum phase transitions between insulating phases. The extended Hubbard model at half-filling with an on-site ( $U$ ) and a nearest neighbor ( $V$ ) Coulomb repulsion provides a prominent example with a transition from a Mott insulator (MI) to a CDW insulator in the vicinity of the  $U = 2V$  line in the phase diagram [4]. Remarkably, the transition involves an intermediate phase with a bond-order wave (BOW) [5,6].

In recent years particular attention has been given to another example for an extension of the Hubbard model which includes a staggered potential term [7–9]. The corresponding Hamiltonian has been named the “ionic Hubbard model” (IHM); at half-filling this model undergoes a different kind of insulator-insulator transition from a band to a correlated Mott-Hubbard type insulator. Conflicting results have so far been reported regarding the nature of the transition, the possibility of two rather than one critical point, or the appearance of BOW order [10,8,9,11–13]. Given the numerous unresolved issues

we reinvestigate in detail the IHM using both, numerical and analytical tools. Specifically we study the 1D Hamiltonian

$$H = -t \sum_{i,\sigma} (1 + (-1)^i \delta) (c_{i\sigma}^\dagger c_{i+1\sigma} + H.c.) + U \sum_i n_{i\uparrow} n_{i\downarrow} + \frac{\Delta}{2} \sum_{i\sigma} (-1)^i n_{i\sigma} \quad , \quad (1)$$

where  $c_{i\sigma}^\dagger$  creates an electron on site  $i$  with spin  $\sigma$ ,  $n_{i\sigma} = c_{i\sigma}^\dagger c_{i\sigma}$ .  $\Delta$  is the potential energy difference between neighboring sites, and  $\delta$  a Peierls modulation of the hopping amplitude  $t$ . In the limit  $\Delta = \delta = 0$ , Eq. (1) reduces to the ordinary Hubbard model, the limit  $\Delta = 0$  and  $\delta > 0$  is called the Peierls-Hubbard model (PHM), and the limit  $\Delta > 0$  and  $\delta = 0$  is usually referred to as the IHM. In the following, we will focus mainly on the effect of the on-site modulation  $\Delta$ , so we implicitly assume  $\delta = 0$  except where stated otherwise.

The IHM was first proposed and discussed almost 20 years ago in the context of organic mixed-stack charge-transfer crystals with alternating donor ( $D$ ) and acceptor ( $A$ ) molecules ( $\dots D^{+\rho} A^{-\rho} \dots$ ) [14,7]. These stacks form quasi-1D insulating chains, and are classified into two categories depending on the amount of charge transfer  $\rho$ : quasi-neutral for  $\rho < 0.5$ , and quasi-ionic for  $\rho > 0.5$ . Torrance *et al.* [14] found that at room temperature and ambient pressure, these materials are either mostly ionic ( $\rho \approx 1$ ) or mostly neutral ( $\rho \approx 0$ ), but several systems undergo a reversible neutral to ionic phase transition (NIT) [15], i.e. a discontinuous jump in the ionicity  $\rho$  upon changing temperature or pressure with the simultaneous appearance of a Peierls lattice distortion [16,17]. The original modelling of the NIT in charge-transfer salts included different Coulomb repulsion parameters on A and D molecules as well as intersite interactions [18,19] and electron-molecular vibration coupling [20]. In these extended ionic Hamiltonians the NIT was found to be first or second order depending on the relative strengths of the different interactions.

In addition, the IHM has been used in a quite different context to describe the ferroelectric transition in perovskite materials such as BaTiO<sub>3</sub> [21,22,10] or KNbO<sub>3</sub> [24]. The IHM here is used as a simple model for a binary compound,  $AB$ , with the  $A$  sites representing the transition metal element (e.g. Ti), and the  $B$  sites representing the oxygen. The staggered potential in this case is the energy difference of the levels on the  $A$  and  $B$  sites [21,22].

The results of our work on the IHM support the existence of a single transition at a critical coupling  $U_c(\Delta)$  from a band- to a correlated insulator (CI) phase. The transition originates from a ground-state level crossing with a change of the site-parity eigenvalue. From our results we identify the strong coupling phase at  $U > U_c(\Delta)$  as a CI with long-range CDW order. Two possibilities arise for the unconventional CI phase: it either has a vanishing spin excitation gap and exhibits on top of a CDW pattern an identical power law decay of SDW and dimer-dimer correlations; or the spin gap remains finite in the CI phase with true long range BOW order coexisting with a CDW. Within the achievable numerical accuracy our data support the latter scenario. Furthermore, we provide the first numerical evaluation of the optical conductivity for the IHM which allows for an additional characterization of the "metallic" transition point  $U_c(\Delta)$  where the optical gap closes. The distinction between charge and optical gaps is crucial for the structure of the ground-state phase diagram.

The outline of our paper is as follows: In sections II and III we summarize previously proposed scenarios for the ground-state phase diagram using bosonization and symmetry arguments. Section IV contains a detailed reanalysis of the bosonization approach to the IHM. In sections V and VI we present our numerical Lanczos and DMRG results, from which we draw conclusions for the ground state phase diagram, and in section VII we discuss dynamical DMRG results for the optical conductivity. Finally, we conclude and summarize in section VIII.

## II. INSULATOR-INSULATOR TRANSITION

A good starting point for understanding the existence of a phase transition in the IHM is the atomic limit [25,9]. For  $t = 0$ , it is immediately seen that at half-filling and  $U < \Delta$  the ground-state of the IHM has two electrons on the odd sites, and no electrons on the even sites corresponding to CDW ordering with maximum amplitude. On the other hand, for  $U > \Delta$  each site is occupied by one electron. Obviously, for  $t = 0$  a transition occurs at a critical value  $U_c = \Delta$ . This transition is expected to persist for finite hopping amplitudes  $t > 0$ , where the alternating potential still defines two sublattices, doubling the unit cell and opening up a band gap  $\Delta$  for  $U = 0$  at  $k = \pm\pi/2$ . For  $t > 0$  the critical coupling shifts to  $U_c(t) > \Delta$ , where  $U_c$  increases monotonically with in-

creasing  $\Delta$ . For  $U, \Delta \gg t$  the system is close to the atomic limit, and  $U_c$  approaches  $\Delta$  from above.

For  $U = 0$  the ground state at half-filling is a CDW band insulator (BI), whose elementary spectrum consists of particle-hole excitations over the band gap. We consider a system to be in a BI phase when the criterion  $\Delta_S = \Delta_C$  holds, where the spin ( $\Delta_S$ ) and the charge gap ( $\Delta_C$ ) are given by

$$\begin{aligned} \Delta_S &= E_0(N = L, S_z = 1) - E_0(N = L, S_z = 0), \\ \Delta_C &= E_0(N = L + 1, S_z = 1/2) \\ &\quad + E_0(N = L - 1, S_z = 1/2) - 2E_0(N = L, S_z = 0). \end{aligned}$$

$E_0(N, S_z)$  is the ground-state energy,  $L$  the system length,  $N$  the number of electrons, and  $S_z$  the  $z$ -component of the total spin. For  $U > U_c$  and  $U \gg t, \Delta$ , the charge gap is set by the Coulomb interaction  $U$ , and the system is a CI with  $\Delta_C > \Delta_S$ . However, in contrast to the cases with  $\Delta = 0$  or  $t = 0$ , CDW order is expected for all finite values of  $U$ .

The IHM is distinctly different from the PHM. This is also a BI at  $U = 0$ , but in contrast to the IHM has  $\Delta_C > \Delta_S > 0$  for any value of  $U > 0$ , i.e. the phase transition from the Peierls BI to the CI occurs at  $U_c = 0$ .

A renewal of interest in the IHM started with the bosonization analysis of Fabrizio *et al.* (FGN) [8] and exact diagonalization studies [9], where a new scenario for the intermediate region  $U \approx \Delta$  was proposed. Several subsequent numerical treatments of the model [27,28,11–13] led to partially contradicting results. Different conclusions were reached about the nature of the insulator-insulator phase transition, the possible existence of two transitions, and the question whether the spin gap closes in the strong coupling phase.

FGN argued that for small but finite  $U$  the BI persists up to a critical value  $U_{c1}$ , where  $\Delta_C = 0$  and the system might be "metallic". Upon further increasing  $U$  they predicted a "spontaneously dimerized", (SDI or equivalently a BOW) intermediate phase, which should undergo a continuous transition into the MI phase at a second critical value  $U_{c2} > U_{c1}$ . A BOW ground state is characterized by long-range staggered bond-density correlations

$$g_B(r) = \frac{1}{L} \sum_i \langle \psi_0 | B_i B_{i+r} | \psi_0 \rangle, \quad (2)$$

$$B_i = \sum_{\sigma} \left( c_{i\sigma}^{\dagger} c_{i+1\sigma} + H.c. \right) \quad (3)$$

and implies a finite spin gap  $\Delta_S > 0$ .

Evidence for such a BOW state has been reported by Wilkens and Martin in a quantum Monte Carlo (QMC) study [11]. More precisely, the authors of Ref. [11] observed a single transition from the BI to the correlated BOW phase. On the contrary, DMRG results [28] and Lanczos studies of level crossings in the excitation spectra support the existence of two transitions with an intervening BOW state [13]. From finite size extrapolations

it was furthermore concluded that  $\Delta_S = 0$  above the critical region [10,26,28]. Whether CDW order persists also in the strong coupling regime remained unsettled in previous work.

### III. SYMMETRY ANALYSIS

Insight into the nature of the BI-MI transition is obtained from a symmetry analysis. The IHM is invariant with respect to *inversion* at a site and *translation* by two lattice sites. Thus, any nondegenerate eigenstate of  $H$  is also an eigenstate of the operators that generate the corresponding symmetry transformation. If we denote the site inversion operator by  $P$ , defined through

$$Pc_{i\sigma}^\dagger P^\dagger = c_{L-i\sigma}^\dagger \quad \text{for } i = 0, \dots, L-1, \quad (4)$$

and  $\hat{T}_j$  for a translation by  $j$  sites, then any nondegenerate eigenstate  $|\psi_n\rangle$  of  $H$  must obey  $P|\psi_n\rangle = \pm|\psi_n\rangle$  and  $\hat{T}_2|\psi_n\rangle = |\psi_n\rangle$ . Because  $[H, \hat{T}_1] \neq 0$ , a non-degenerate eigenstate  $|\psi_n\rangle$  of  $H$  can not be an eigenstate of  $\hat{T}_1$ .

For the half-filled Hubbard model ( $\Delta = \delta = 0$ ) the site-parity eigenvalue of the ground state can be determined in the limits  $U = 0$  and  $U \gg t$  [9]. For  $U = 0$ , the ground state is a direct product of spin up and spin down Slater determinants, both formed from the same occupied spatial wavefunctions with the same parity  $P_\sigma = \pm 1$ , so the parity eigenvalue of the total wavefunction is given by their product  $P = P_\uparrow \times P_\downarrow = \pm 1$ . Hence, the state at  $U = 0$  is even under site inversion. On the other hand, in the large  $U$  limit the mapping to the Heisenberg Hamiltonian can be used to show that for  $L = 4n$  with periodic boundary conditions (PBC) or  $L = 4n + 2$  with antiperiodic boundary conditions (APBC) the ground state obeys  $P|\psi_0\rangle = -|\psi_0\rangle$  (for details see [9]). In finite chains, these combinations of chain lengths and boundary conditions ensure that  $k = \pi/2$  is an allowed momentum in the Brillouin zone (BZ). This is important at half-filling, where  $k = \pm\pi/2$  is the BZ boundary. It follows that upon increasing the number of sites  $L$ , the ground state for  $U \gg t$  will be odd with respect to  $P$  as long as  $k = \pi/2$  is an allowed  $k$  value, and this feature will persist in the thermodynamic limit  $L \rightarrow +\infty$ . For the ordinary Hubbard model the discrete inversion symmetry changes therefore between  $U = 0$  and  $U \gg t$ . Since the model has no phase transition for  $U > 0$ , the ground state has  $P = +1$  only for  $U = 0$ , and  $P = -1$  for any  $U > 0$ .

However, in the IHM the phase transition from a BI to a CI occurs at some finite  $U_c > 0$ . This suggests that the parity of the ground state remains even not only for  $U = 0$ , but for all  $U < U_c$ . At  $U_c$ , a ground-state level crossing occurs on finite chains, as confirmed by exact diagonalization studies (see below), connected with a site-parity change.

In the strong-coupling limit, the IHM was argued in some previous treatments [9,8,13] to be a MI with  $\Delta_S =$

0. For the IHM with  $U \gg t, \Delta$  the effective Heisenberg spin model

$$H_{eff} = J \sum_i \mathbf{S}_i \cdot \mathbf{S}_{i+1} + J' \sum_i \mathbf{S}_i \cdot \mathbf{S}_{i+2} \quad (5)$$

was derived to describe the low-energy physics [7]. In Eq. (5) the exchange couplings are given by

$$J = \frac{4t^2}{U} \left[ \frac{1}{1-x^2} - \frac{4t^2}{U^2} \frac{1+4x^2-x^4}{(1-x^2)^3} \right],$$

$$J' = \frac{4t^4}{U^3} \frac{(1+4x^2-x^4)}{(1-x^2)^3}, \quad (6)$$

where  $x = \Delta/U$ . It is important to recall that in the derivation of the effective spin model the Hilbert space of the IHM is divided into two subspaces – one containing no doubly occupied sites, and one containing all states with at least one doubly occupied site. The atomic limit of the IHM is taken as the unperturbed problem  $H_0$ , and the kinetic term in (1) is treated as a perturbation. The ground state of  $H_0$  is therefore in the subspace without double occupancies. The kinetic term lifts the spin degeneracy in this subspace. Introducing the projection operator  $P = \prod_i (1 - n_{i\uparrow}n_{i\downarrow})$ , the effective Hamiltonian  $H_{eff} = P \exp(iS) H \exp(-iS) P$  is obtained by a canonical transformation  $S$  and an expansion in powers of  $t/U$  around  $H_0$  [29,30].

The result (5) would imply that in the strong-coupling limit of the IHM the low-energy physics is qualitatively similar to that of the Hubbard model, with modified exchange coupling constants  $J$  and  $J'$ . For next-nearest neighbor couplings  $J' < 0.24J$  the spin gap vanishes [31]; thus the system would be a true MI. The coupling constants (6) satisfy the condition  $J' < 0.24J$  at least for  $U > 3.6t$  for  $\Delta \leq t$  and  $U > 3.6\Delta$  for  $\Delta > t$ . However, the effective model (5) is invariant with respect to translations by *one* lattice spacing, whereas the original IHM is invariant only with respect to translations by *two* lattice spacings. Thus, the effective spin Hamiltonian has a higher symmetry than the original model from which it was derived, and the arguments of the strong-coupling expansion in favor of  $\Delta_S = 0$  for  $U > U_c$  cannot be considered rigorous as was also pointed out in Ref. [11].

Of course, also in the Hubbard chain for any  $U < \infty$  the double occupancy is not zero. However, these “virtual doublons” are distributed equally over all sites, and therefore do not change the translational symmetry. If only the spin excitations are considered, these doublons are never traced.

As originally discussed in Ref. [19] the existence of a level crossing on finite chains at a critical  $U_c$  leaves the following possibilities for the ground state of the IHM at  $U > U_c$  in the thermodynamic limit: 1. The ground state remains unique with site-parity quantum number  $P = -1$ . This necessarily implies the absence of BOW and the system is in the MI phase with a vanishing spin

gap and absence of long range CDW. Remarkably and left uncommented before, this scenario implies the highly unusual situation that the strong coupling ground state has a higher symmetry than the IHM Hamiltonian. 2. The ground state is twofold degenerate and supports a long-range BOW+CDW order. This possibility requires the spin gap to remain finite [8]. These intimately connected properties are violated in the conclusions reached in Ref. [12]. This second scenario though still allows for an additional second transition into the MI phase as characterized in 1.

#### IV. BOSONIZATION RESULTS

The standard bosonization procedure allows to express the Hamiltonian density in the following way [8]:  $\mathcal{H} = \mathcal{H}_c + \mathcal{H}_s + \mathcal{H}_{cs}$ , where the charge and spin degrees of freedom are represented by a sine-Gordon model for scalar fields  $\phi_c$  and  $\phi_s$ , respectively:

$$\mathcal{H}_c = \frac{v_c}{2} [P_c^2(x) + (\partial_x \phi_c)^2] - \frac{U}{2\pi a_0^2} \cos(\sqrt{8\pi K_c} \phi_c(x)), \quad (7)$$

$$\mathcal{H}_s = \frac{v_s}{2} [P_s^2(x) + (\partial_x \phi_s)^2] + \frac{U}{2\pi a_0^2} \cos(\sqrt{8\pi} \phi_s(x)); \quad (8)$$

$a_0$  is the lattice constant. The ionic term determines the spin-charge coupling

$$\mathcal{H}_{cs} = \frac{\Delta}{\pi a_0} \sin(\sqrt{2\pi K_c} \phi_c(x)) \cos(\sqrt{2\pi} \phi_s(x)). \quad (9)$$

Here  $P_{c(s)}(x)$  is the momentum conjugate to  $\phi_{c(s)}(x)$ ,  $v_{c(s)}$  is the velocity of charge (spin) excitations and  $K_c \simeq 1 - U/4\pi t$ . This means that the model (13) is in a strong-coupling regime for arbitrary  $U > 0$ , and at  $\Delta = 0$  the dynamically generated mass determines the charge gap in the system.

##### A. Forward scattering model with ionic and/or Peierls distortion

We first consider the limit of a weak Hubbard interaction  $U \ll \Delta \ll t$ , where the properties of the system are mostly determined by the ionic distortion. In the infrared (low energy - large distance) limit the Umklapp and backward scattering processes, described in Eqs. (7)-(8) by the terms  $U \cos(\sqrt{8\pi K_c} \phi_c(x))$  and  $U \cos(\sqrt{8\pi} \phi_s(x))$ , respectively, are frozen out. Therefore, we initially neglect these terms and consider the Hamiltonian

$$\mathcal{H}_{TL} = \int dx \left\{ \frac{v_c}{2} [P_c^2(x) + (\partial_x \phi_c)^2] \right\} \quad (10)$$

$$+ \int dx \left\{ \frac{v_s}{2} [P_s^2(x) + (\partial_x \phi_s)^2] \right\} - \frac{\Delta}{\pi a_0} \int dx \sin(\sqrt{2\pi K_c} \phi_c) \cos(\sqrt{2\pi K_s} \phi_s),$$

i.e. the half-filled Tomonaga-Luttinger (TL) model with ionic distortion. The non-interacting system corresponds to the particular limit  $K_c = K_s = 1$ . For generality we do not assume  $SU(2)$  symmetry of the spin channel and therefore the parameter  $K_s$  is not fixed to unity.

If we decouple the interaction term in a mean-field manner by introducing

$$m_c = \Delta \cdot \langle \cos(\sqrt{2\pi K_s} \phi_s) \rangle, \quad (11)$$

$$m_s = \Delta \cdot \langle \sin(\sqrt{2\pi K_c} \phi_c) \rangle, \quad (12)$$

the bosonized Hamiltonian reads  $\mathcal{H} = \mathcal{H}_c + \mathcal{H}_s$  where

$$\mathcal{H}_c = \int dx \left\{ \frac{v_c}{2} [P_c^2(x) + (\partial_x \phi_c)^2] - \frac{m_c}{\pi a_0} \sin(\sqrt{2\pi K_c} \phi_c) \right\}, \quad (13)$$

$$\mathcal{H}_s = \int dx \left\{ \frac{v_s}{2} [P_s^2(x) + (\partial_x \phi_s)^2] - \frac{m_s}{\pi a_0} \cos(\sqrt{2\pi K_s} \phi_s) \right\}. \quad (14)$$

We can estimate the renormalized masses as

$$M_c \simeq \Lambda \left( \frac{m_c}{\Lambda} \right)^{2/(4-K_c)}, \quad (15)$$

$$M_s \simeq \Lambda \left( \frac{m_s}{\Lambda} \right)^{2/(2-K_s)}, \quad (16)$$

where  $\Lambda$  is a cut-off energy. Similarly, the expectation values of  $\sin(\sqrt{2\pi K_c} \phi_c)$  and  $\cos(\sqrt{2\pi K_s} \phi_s)$  are estimated as

$$\langle \sin(\sqrt{2\pi K_c} \phi_c) \rangle \simeq \left( \frac{m_c}{\Lambda} \right)^{K_c/(4-K_c)}, \quad (17)$$

$$\langle \cos(\sqrt{2\pi K_s} \phi_s) \rangle \simeq \left( \frac{m_s}{\Lambda} \right)^{K_s/(4-K_s)}. \quad (18)$$

The self-consistency equation

$$\Delta = \frac{m_c}{\langle \sin(\sqrt{2\pi K_s} \phi_s) \rangle} = \frac{m_s}{\langle \sin(\sqrt{2\pi K_c} \phi_c) \rangle} \quad (19)$$

leads to

$$\frac{m_s}{\Lambda} = \left( \frac{m_c}{\Lambda} \right)^{(4-K_s)/(4-K_c)}. \quad (20)$$

Using Eqs. (11)-(19) one easily finds that

$$M_s = M_c = \Lambda \left( \frac{\Delta}{\Lambda} \right)^{2/(4-K_c-K_s)},$$

and the system is a BI with a weakly renormalized value of the excitation gap. In particular, for the non-interacting system  $K_c = K_s = 1$  and  $M_s = M_c = \Delta$ .

For the PHM the bosonized expression for the Peierls distortion term is given by

$$-\frac{\delta}{\pi a_0} \cos(\sqrt{2\pi}\phi_c) \cos(\sqrt{2\pi}\phi_s). \quad (21)$$

By following again the same steps as above the half-filled TL model with a Peierls distortion also exhibits the properties of a BI with equal charge and spin gaps.

### B. Renormalization effects from the short-range interaction

In order to account for the renormalization of the BI gap by the short-range part of the interaction, we consider again the limiting case  $U \ll \Delta \ll t$ . We treat both the ionic term and the Hubbard interaction on the same footing in a perturbative way. For this purpose it is convenient to consider the 2D Euclidean action:

$$S = S_0 + S_{int}, \quad (22)$$

$$S_0 = v_F \int d^2\mathbf{x} \left\{ \frac{1}{2} [(\nabla\phi_c)^2 + (\nabla\phi_s)^2] \right\},$$

$$S_{int} = v_F \int d^2\mathbf{x} \left\{ \frac{m_{cs}}{\pi a_0} \sin(\sqrt{2\pi K_c}\phi_c) \cos(\sqrt{2\pi}\phi_s) + \frac{M_c}{\pi a_0^2} \cos(\sqrt{8\pi K_c}\phi_c) + \frac{M_s}{\pi a_0^2} \cos(\sqrt{8\pi}\phi_s) \right\}.$$

Here the dimensionless coupling constants are given by

$$M_c = -\frac{U}{4\pi t}, \quad M_s = \frac{U}{4\pi t}, \quad m_{cs} = -\frac{\Delta}{2\pi t}. \quad (23)$$

Expanding the partition function

$$Z = \int D\Phi_s D\Phi_c e^{-S_0[\Phi_c, \Phi_s]} [1 - S_{int} + \frac{1}{2} S_{int}^2 + \dots] \quad (24)$$

we integrate out all configurations in the second order term with  $|\mathbf{x} - \mathbf{x}'| \sim a_0$ . Using the operator product expansion formulas

$$\int \frac{d^2\mathbf{x}}{a_0^2} \int \frac{d^2\mathbf{x}'}{a_0^2} \sin(\phi(\mathbf{x})) \cdot \cos(2\phi(\mathbf{x}')) = -\frac{\pi}{2} \int \frac{d^2\mathbf{x}}{a_0^2} [\sin(\phi_c(\mathbf{x})) + \dots], \quad (25)$$

$$\int \frac{d^2\mathbf{x}}{a_0^2} \int \frac{d^2\mathbf{x}'}{a_0^2} \cos(\phi(\mathbf{x})) \cdot \cos(2\phi(\mathbf{x}')) = +\frac{\pi}{2} \int \frac{d^2\mathbf{x}}{a_0^2} [\cos(\phi_c(\mathbf{x})) + \dots], \quad (26)$$

$$\int \frac{d^2\mathbf{x}}{a_0^2} \int \frac{d^2\mathbf{x}'}{a_0^2} \cos(\phi(\mathbf{x})) \cdot \cos(\phi(\mathbf{x}')) = +\frac{\pi}{2} \int \frac{d^2\mathbf{x}}{a_0^2} [1 - \frac{1}{2}(\nabla\phi_c)^2 + \cos(2\phi(\mathbf{x})) + \dots], \quad (27)$$

$$\int \frac{d^2\mathbf{x}}{a_0^2} \int \frac{d^2\mathbf{x}'}{a_0^2} \sin(\phi(\mathbf{x})) \cdot \sin(\phi(\mathbf{x}')) = +\frac{\pi}{2} \int \frac{d^2\mathbf{x}}{a_0^2} [1 - \frac{1}{2}(\nabla\phi_c)^2 - \cos(2\phi(\mathbf{x})) + \dots], \quad (28)$$

where dots denote strongly irrelevant terms of higher critical dimensionality, we obtain the following renormalization of the model parameters:

$$\tilde{\Delta} = \Delta \left( 1 - \lambda \frac{U}{t} \right), \quad (29)$$

$$\tilde{M}_c = -U \left( 1 - \lambda_c \frac{\Delta^2}{Ut} \right), \quad (30)$$

$$\tilde{M}_s = U \left( 1 - \lambda_s \frac{\Delta^2}{Ut} \right). \quad (31)$$

$\lambda$ ,  $\lambda_c$ , and  $\lambda_s$  are positive numbers of order unity. We observe that

- the parameter of the ionic distortion is renormalized linearly by the on-site repulsion;
- the amplitudes of the Umklapp and backward scattering processes ( $\tilde{M}_c$  and  $\tilde{M}_s$ , respectively) are renormalized quadratically by the ionic distortion;
- the  $U \leftrightarrow -U$  asymmetry of the model is clearly manifested: at  $U > 0$  the amplitude of the strongly relevant Umklapp scattering decreases, while at  $U < 0$  the amplitude of the strongly relevant backscattering processes increases.

Therefore we conclude that in the IHM the BI phase is more stable for a repulsive than an attractive Hubbard interaction.

For a Peierls distortion the effect of the electron-electron interaction at short distances is rather different. Assuming  $U \ll \delta \ll t$  the same procedure as above gives in this case the following expressions for the renormalized parameters

$$\tilde{\delta} = \delta \left( 1 + O\left(\frac{U}{t}\right)^2 \right), \quad (32)$$

$$\tilde{M}_c^P = -U \left( 1 + \lambda'_c \frac{\delta^2}{Ut} \right), \quad (33)$$

$$\tilde{M}_s^P = U \left( 1 - \lambda'_s \frac{\delta^2}{Ut} \right). \quad (34)$$

Therefore, contrary to the ionic case,

- the amplitude of the Peierls distortion is not renormalized to linear order in  $U$ ;
- the amplitudes of the Umklapp and backward scattering processes are renormalized quadratically by the Peierls distortion term;
- at  $U > 0$  the amplitude of the strongly relevant Umklapp scattering increases, while at  $U < 0$  the amplitude of the strongly relevant backscattering processes increases.

Based on these arguments, one is led to predict that for the PHM the deviation from the BI behavior due to

the on-site coupling of arbitrary sign could be similar to that of the attractive IHM.

Therefore we conclude that the BI phase in the Peierls-Hubbard model is less stable against a Peierls distortion which is not renormalized to linear order in  $U$ , and the amplitudes of the relevant scattering processes  $M_c^P$  at  $U > 0$  and  $M_s^P$  at  $U < 0$  always increase. The deviation from the BI behavior in the case of the attractive IHM and the PHM should therefore happen almost at the same values of the on-site interaction. The fundamentally different behavior of the repulsive IHM and the PHM will indeed be verified below.

### C. The FGN phase diagram

In Ref. [8] FGN proposed a new scenario for the BI to MI crossover in the IHM. The key ingredient of their theory is the presence of *two separate transitions*: an Ising-type transition at  $U_{ch}^c$  where the charge gap vanishes and a continuous transition at  $U_{sp}^c > U_{ch}^c$  where the spin gap vanishes. The charge excitations are gapped for arbitrary  $U \neq U_{ch}^c$ , while the spin sector remains gapless at  $U > U_{sp}^c$ . The ground-state phase diagram of the IHM and the properties of the charge and spin gapped phases were argued to be qualitatively captured by the effective potential:

$$\mathcal{V}(\phi_c, \phi_s) = -\tilde{\Delta} \sin(\sqrt{2\pi K_c} \phi_c) \cos(\sqrt{2\pi} \phi_s) - \tilde{M}_c \cos(\sqrt{8\pi K_c} \phi_c) - \tilde{M}_s \cos(\sqrt{8\pi} \phi_s), \quad (35)$$

where  $\tilde{M}_c, \tilde{M}_s, \tilde{\Delta} > 0$  are phenomenological parameters obtained by integrating out high-energy excitations. Minimizing  $\mathcal{V}(\phi_c, \phi_s)$  with respect to  $\phi_c$  and  $\phi_s$  results in the following sets of vacua: For  $\tilde{\Delta} > 4\tilde{M}_c$  (i.e.  $U < U_{ch}^c$ )

$$\begin{aligned} \text{I. } & \sqrt{2\pi} \phi_s = 2\pi n, \quad \sqrt{2\pi K_c} \phi_c = \frac{\pi}{2} \pmod{2\pi} \\ \text{II. } & \sqrt{2\pi} \phi_s = \pi + 2\pi n, \quad \sqrt{2\pi K_c} \phi_c = -\frac{\pi}{2} \pmod{2\pi} \end{aligned} \quad (36)$$

while for  $\tilde{\Delta} < 4\tilde{M}_c$  (i.e.  $U_{ch}^c < U < U_{sp}^c$ )

$$\begin{aligned} \text{I. } & \sqrt{2\pi} \phi_s = 2\pi n, \quad \sqrt{2\pi K_c} \phi_c = \varphi_0, \quad \pi - \varphi_0 \pmod{2\pi} \\ \text{II. } & \sqrt{2\pi} \phi_s = \pi + 2\pi n, \\ & \sqrt{2\pi K_c} \phi_c = -\varphi_0, \quad -\pi + \varphi_0 \pmod{2\pi} \end{aligned} \quad (37)$$

where  $\varphi_0 = \arcsin(\tilde{\Delta}/4\tilde{M}_c)$ .

The symmetry properties of the various ordered phases are described by the order parameters for the short wavelength fluctuations of the

- *site-located charge density wave*:

$$\begin{aligned} \Delta_{CDW} &= (-1)^n \sum_{\sigma} c_{n,\sigma}^{\dagger} c_{n,\sigma} \\ &\sim \sin(\sqrt{2\pi K_c} \phi_c) \cos(\sqrt{2\pi} \phi_s) \end{aligned} \quad (38)$$

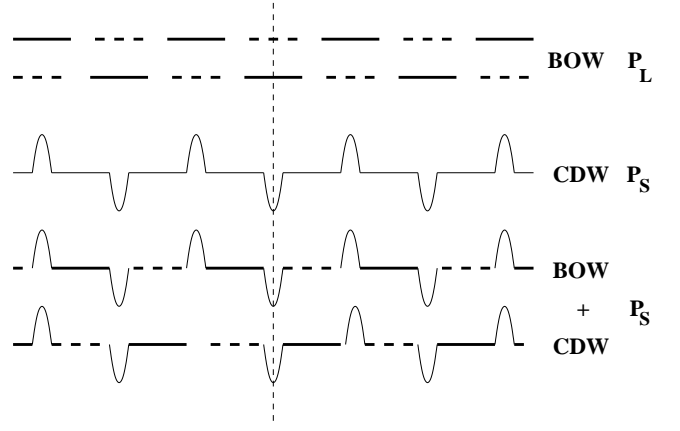


FIG. 1. Illustration of the CDW + BOW phase. Top figure: two degenerate dimerization patterns; the vertical dashed line is a mirror axis indicating the link-reflection symmetry of each dimer state. Middle figure: schematic representation for a staggered CDW which has site-reflection symmetry. Lower figure: the superposition of the CDW state with both dimerized patterns again allows for a site-reflection symmetric state.

- *site-located spin density*:

$$\begin{aligned} \Delta_{SDW} &= (-1)^n \sum_{\sigma} \sigma \rho_{n,\sigma} \\ &\sim \cos(\sqrt{2\pi K_c} \phi_c) \sin(\sqrt{2\pi} \phi_s), \end{aligned} \quad (39)$$

- *bond-located charge density wave*:

$$\begin{aligned} \Delta_{BOW} &= (-1)^n \sum_{\sigma} (c_{n,\sigma}^{\dagger} c_{n+1,\sigma} + h.c.) \\ &\sim \cos(\sqrt{2\pi K_c} \phi_c) \cos(\sqrt{2\pi} \phi_s). \end{aligned} \quad (40)$$

For  $U < U_{ch}^c$  the charge and spin excitation spectra are gapped. The vacuum values of the ordered fields are  $\langle \phi_s \rangle = 0$  and  $\langle \phi_c \rangle = \sqrt{\pi/8K_c}$  and the system has long-range CDW order. Thus the set of vacua (36) corresponds to the BI phase.

For  $U_{ch}^c < U < U_{sp}^c$  the vacuum expectation values of the ordered charge field is now different:  $\langle \phi_s \rangle = 0$  and  $\langle \sqrt{2\pi K_c} \phi_c \rangle = \varphi_0$ . In this phase, long-range CDW and BOW correlations coexist,

$$\begin{aligned} \langle \Delta_{CDW}(x) \Delta_{CDW}(x') \rangle &\sim \sin^2 \varphi_0, \\ \langle \Delta_{BOW}(x) \Delta_{BOW}(x') \rangle &\sim \cos^2 \varphi_0. \end{aligned}$$

The standard BOW phase violates site- but preserves link-inversion symmetry. In the CDW + BOW phase, due to the CDW pinning by the ionic distortion, the link-parity is also broken. However, in the absence of an externally imposed Peierls distortion, the BOW pattern is doubly degenerate. Thus the charge distribution in the CDW + BOW phase can be represented as a linear combination of two dimerized patterns shifted with respect to each other by one lattice spacing (see Fig. 1) for which the site-inversion symmetry is not broken.

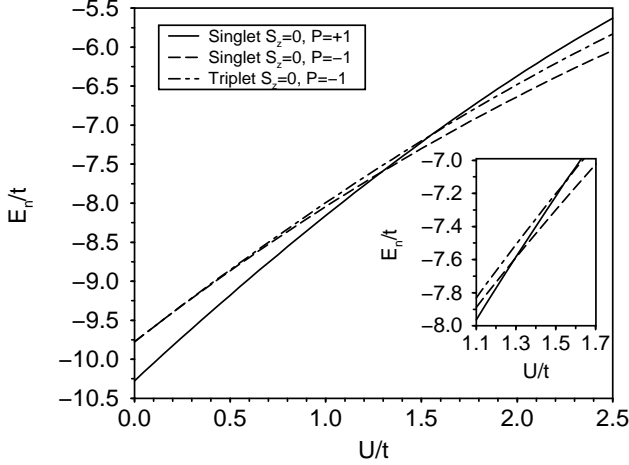


FIG. 2. Lowest energy eigenvalues of the IHM at half-filling for  $L = 8$  sites, periodic boundary conditions and  $\Delta = 0.5t$ .

Finally, at  $U > U_{sp}^c$  the spin gap disappears. According to FGN at this point  $\varphi_0 = 0$  and the standard MI phase, with an identical power-law decay of the SDW and Peierls correlations is realized.

However, the results of our numerical studies presented below as well as QMC calculations [11] and finite cluster studies using valence bond techniques [12] indicate a different scenario. The amplitude of the CDW correlations smoothly decays with increasing  $U$  with  $\varphi_0 \rightarrow 0$  for  $U \rightarrow \infty$ .

## V. LANCZOS EXACT DIAGONALIZATION RESULTS

In order to explore the nature of the spectrum and the phase transition, we have diagonalized numerically small systems by the Lanczos method [33] extending earlier exact diagonalization calculations [10,9]. The energies of the few lowest eigenstates were obtained for finite chains with  $L = 4n$  and PBC or  $L = 4n + 2$  with APBC, for reasons discussed above.

We first analyze a short chain without finite-size scaling. For chain lengths  $L \leq 16$  finite-size effects do not change the qualitative behavior discussed below. In Fig. 2, the lowest eigenenergies of the IHM for  $\Delta = 0.5t$ ,  $L = 8$  and PBC are shown as a function of  $U$ . At  $U = 1.3t$ , a level crossing of the two lowest eigenstates occurs. A non-degenerate eigenstate of the IHM has site-parity eigenvalues  $\pm 1$ , so a ground state level-crossing transition corresponds to a change of the site-parity eigenvalue.

For  $U = 0$ , the IHM is easily diagonalized in momentum space by introducing fermionic creation (annihilation) operators  $\gamma_{k\sigma b}^\dagger$  ( $\gamma_{k\sigma b}$ ) with an index  $b = 1, 2$  denoting the lower and upper bands, respectively, giving two energy bands  $E_{1/2}(k) = \pm \sqrt{4 \cos^2(k) + (\Delta/4)^2}$  with

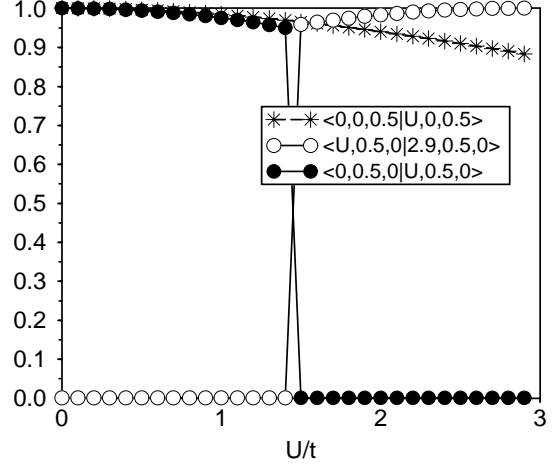


FIG. 3. Overlap matrix elements of the exact ground states  $|\psi_0\rangle = |U/t, \Delta/t, \delta\rangle$  of the Peierls chain ( $U = \Delta = 0$ ) and the Peierls-Hubbard model (stars), the ionic band insulator ( $\Delta = 0.5t$ ,  $\delta = 0$ ) and the IHM (full circles) and of the IHM at a given  $U$  and at  $U = 2.9t$  (circles) as a function of  $U$ . Calculations were performed for 10 sites with antiperiodic boundary conditions.

momenta  $-\pi/2 < k \leq \pi/2$ . For  $U = 0$  the first two degenerate excited states at half-filling always have negative site parity, because the ground state has  $P = +1$ , and the operator  $\gamma_{q\sigma 2}^\dagger \gamma_{q\sigma 1}$  with  $q = \pi/2$  obeys

$$P \gamma_{q\sigma 2}^\dagger \gamma_{q\sigma 1} = -\gamma_{q\sigma 2}^\dagger \gamma_{q\sigma 1} P \quad . \quad (41)$$

The first two excited states shown in Fig. 2 are the spin singlet ( $S = 0$ ,  $S_z = 0$ ) and triplet excitations ( $S = 1$ ,  $S_z = 0$ ), created from the ground state by applying the operators

$$\begin{aligned} & \frac{1}{\sqrt{2}} \left( \gamma_{q\uparrow 2}^\dagger \gamma_{q\uparrow 1} - \gamma_{q\downarrow 2}^\dagger \gamma_{q\downarrow 1} \right) , \\ & \frac{1}{\sqrt{2}} \left( \gamma_{q\uparrow 2}^\dagger \gamma_{q\uparrow 1} + \gamma_{q\downarrow 2}^\dagger \gamma_{q\downarrow 1} \right) , \end{aligned} \quad (42)$$

respectively. Thus both excited states have total momentum  $k_{tot} = 0$  and negative site parity. For  $U > 0$ , these degenerate excited states split in energy.

Fig. 3 shows the overlap matrix elements between the exact ground states  $|\psi_0\rangle = |U/t, \Delta/t, \delta\rangle$  of the IHM, the PHM, and the Hubbard model. Specifically we show the overlap integrals between the ground states of the IHM for  $0 < U < 2.9t$  and  $U = 0$ , and between the ground states for  $0 < U < 2.9t$  and  $U = 2.9t$ . Clearly, a sharp transition occurs at  $U_c = 1.5t$  with the ground states  $|U, 0.5, 0\rangle$  for  $U < U_c$  and  $U > U_c$  being orthogonal to each other. This reflects the level-crossing phenomenon with a site-parity change. For the PHM ( $\Delta = 0$ ,  $\delta = 0.5$ ) the situation is different. The overlap integral between the ground states for  $U = 0$  and  $U > 0$  decreases

continuously with increasing  $U$ , and no indication of a phase transition is observed. This model is a BI only at  $U = 0$ , and turns into a correlated Peierls insulator for any  $U > 0$ .

Obviously, exact diagonalization of finite rings identifies one critical  $U_c > 0$ , separating a BI with  $P = +1$  at  $U < U_c$  from a CI with  $P = -1$  for  $U > U_c$ .

## VI. DMRG RESULTS

In order to access the transition scenario in the long chain-length limit, we have studied chains up to  $L=300$  using the DMRG method [34,35]. The fact that the transition at  $U_c$  is connected with inversion symmetry requires some caution when open boundary conditions (OBC) are used in our DMRG studies. For OBC and  $L = 2n$  the IHM is not reflection symmetric at any site. Thus, the ground state does not have a well defined site-parity, and the level-crossing transition is absent. To overcome this problem, one might try to use chains with OBC and an *odd* number of sites  $L = 2n + 1$ , since the Hamiltonian in this case is reflection-symmetric with respect to the site  $i_c$  in the center of the chain, and a site-parity operator is well defined by

$$P c_{i_c \sigma}^\dagger P^\dagger = c_{L+1-i_c \sigma}^\dagger . \quad (43)$$

To test whether this is an improved choice we have calculated the site-parity of the ground state for  $U = 0$  analytically for different chain lengths  $L = 2n + 1$  and found

$$P|\psi_0\rangle = (-1)^n |\psi_0\rangle . \quad (44)$$

On the other hand, in the large  $U$  limit again the mapping to the Heisenberg Hamiltonian could be used to obtain the site-parity eigenvalue. By extending the idea of Gidopoulos *et al.* [9] to chains with  $L = 2n + 1$ , for  $U \gg t$  we obtain

$$P|\psi_0\rangle = (-1)^{\left[\sum_{m=1}^{L-1} m\right]} |\psi_0\rangle = (-1)^n |\psi_0\rangle . \quad (45)$$

Thus, the parity eigenvalue of the ground state is the same at  $U = 0$  and  $U \gg t$  for a given chain length, and no level crossing occurs. As mentioned above, the argument for  $U \gg t$  requires some caution for the IHM, so we also have checked this result numerically by exact diagonalization of small systems with  $L = 5, 7, 9, \dots$  to confirm the absence of a level crossing. Obviously, results for any choice of boundary conditions should recover the level-crossing scenario when extrapolated to the thermodynamic limit. Due to the fact that the sharp transition at a well defined  $U_c$  does not exist in the finite-chain results for OBC, the extrapolation is a rather subtle problem, since a sharp transition feature has to be identified from the extrapolation of smooth curves. This requires the use of quite long chains in the critical region.

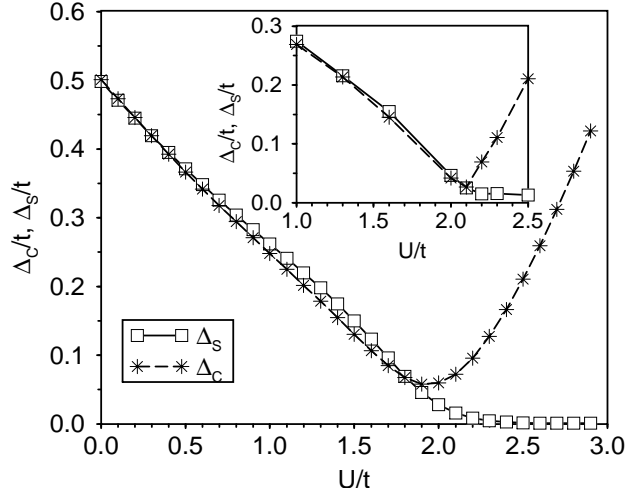


FIG. 4. Results for the spin ( $\Delta_S$ ) and charge ( $\Delta_C$ ) gaps of the IHM at half-filling with  $\Delta = 0.5t$  as a function of  $U$ . Energies were obtained by DMRG calculations on open chains with  $L = \{30, 40, 50, 60\}$  (main plot) and  $L = \{30, 40, 50, 60, 200, 300\}$  (inset), and extrapolated to the limit of infinite chain length.

We have evaluated  $\Delta_C$  and  $\Delta_S$  for chains up to 300 sites. In Fig. 4 extrapolated results are shown as a function of  $U$ . Calculations were performed with OBC for chains of lengths  $L = \{30, 40, 50, 60\}$ , and additionally for  $L = 200$  and  $L = 300$  in the transition region around the estimated  $U_c$ . Unlike the definition (2),  $\Delta_C$  was obtained here using

$$\Delta_C = \frac{1}{2} \left[ E_0(N = L + 2, S_z = 0) + E_0(N = L - 2, S_z = 0) - 2E_0(N = L, S_z = 0) \right].$$

in order to calculate the relevant energies  $E_0$  in the subspace  $S_z = 0$ . This becomes equivalent to (2) in the thermodynamic limit. We assume a scaling behavior of  $\Delta_C$  and  $\Delta_S$  of the form [36]

$$\Delta_i(L) = \Delta_i^\infty + \frac{A_i}{L} + \frac{B_i}{L^2} + \dots , \quad (46)$$

where  $i \in \{S, C\}$ . The extrapolation for  $L \rightarrow \infty$  is then performed by fitting this polynomial in  $1/L$  to the calculated finite-chain results. We note that different finite-size scaling formulas were proposed in the literature mainly when PBC or APBC were used [9].

As can be seen from the main plot in Fig. 4, extrapolating the results for  $L = \{30, 40, 50, 60\}$  does indeed not give a sharp transition behavior of the gaps. As illustrated in the inset, adding results for  $L = 200$  and 300 in the critical region changes the picture considerably. Within numerical accuracy the charge and spin gaps remain equal up to a critical  $U_c \approx 2.1t$ . A sharp

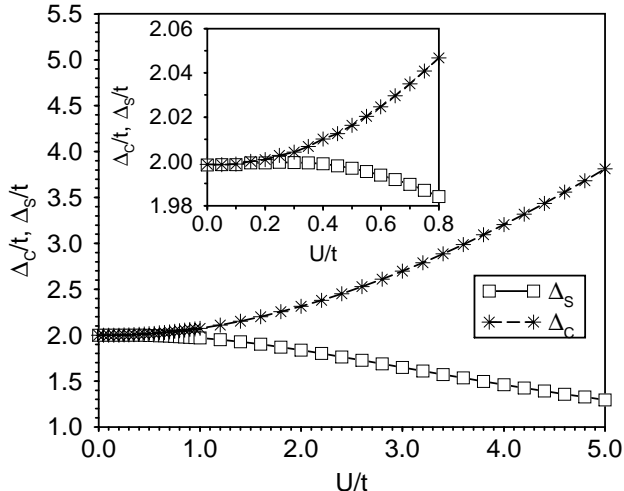


FIG. 5. Results for the spin ( $\Delta_S$ ) and charge ( $\Delta_C$ ) gaps of the Peierls-Hubbard model at half-filling with a modulation of the hopping amplitude  $\delta = 0.5$  as a function of  $U$ . Energies were obtained by DMRG calculations on open chains with  $L = \{30, 40, 50, 60\}$ .

kink for  $\Delta_C$  is observed reflecting the merging of the ground states of the different site-parity sectors. Importantly,  $\Delta_C$  does not close at the critical point. This is in fact not in conflict with an underlying ground-state level crossing. If the ground states of the different site-parity sectors become degenerate, the only rigorous consequence is the closing of the optical excitation gap. The selection rules for optical excitations (see section VII) allow only for transitions between states of different site-parity. Furthermore, optical transitions occur within the same particle number sector. The optical gap is therefore by definition distinct from the charge gap Eq. (2) which involves the removal or the addition of a particle. The critical point  $U_c$  of the IHM corresponds to the remarkable situation where the optical gap closes while  $\Delta_C$  remains finite. This implies that each site-parity sector separately has a finite  $\Delta_C$ . Above  $U_c$  the charge and spin gaps split indicating that the corresponding insulating phase is no longer a BI.  $\Delta_S$  continuously decreases with increasing  $U$  and becomes unresolvably small within the achievable numerical accuracy.

Our results are in general agreement with the data obtained by Qin *et al.* [28]. These authors performed DMRG calculations for the IHM with  $\Delta = 0.6t$ , for chains up to  $L = 600$  sites. In contrast to our calculations, Qin *et al.* used the definition (2) to calculate  $\Delta_C$ . Surprisingly, they observed a non-monotonic scaling behavior of  $\Delta_S$  with  $L$  for values of  $U$  close to the critical  $U_c$ , i.e. for chain lengths  $L > 300$   $\Delta_S$  started to increase again. It remains unclear whether this is due to loss of DMRG accuracy with increasing chain lengths. We note that in their substantially revised paper Qin *et al.* have presented additional DMRG data which agree with our

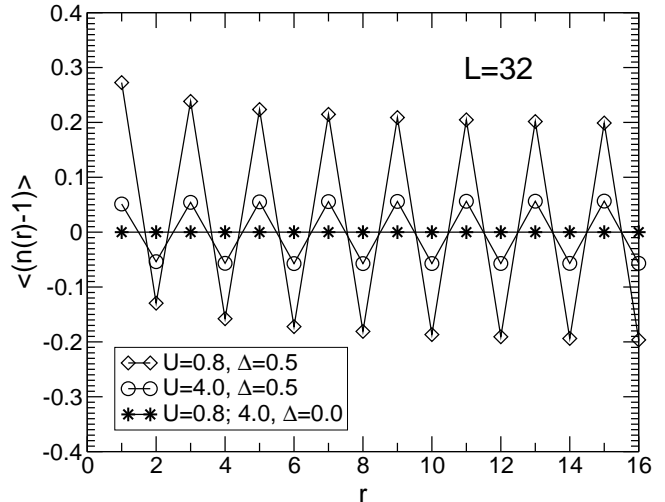


FIG. 6. The electron density distribution in the ground state of the IHM for  $\Delta = 0.5t$  and  $U = 0.8t$  (diamonds) and  $U = 4t$  (circles). Results were obtained by DMRG calculations on open chains with  $L = 32$ . Stars show results for the Hubbard chain ( $\Delta = 0$ ).

present finding. DMRG calculations for the IHM with  $\Delta = t$  have also been performed by Takada and Kido for chains up to  $L = 400$  sites [27]. The authors interpret their results in the region close to  $U_c$  in favour of a two-transition scenario similar to that of FGN [8]. Below we will show that such an interpretation is not valid.

For comparison we show in Fig. 5 the spin and charge gaps versus  $U$  in the PHM. As already anticipated in previous sections this model does not show any signature of a phase transition; i.e.  $\Delta_C > \Delta_S > 0$  for all  $U > 0$ . So although the Peierls and the ionic insulator for  $U = 0$  similarly possess an excitation gap at the BZ boundary, applying a Coulomb  $U$  leads to distinctly different behavior in both cases. The origin of the different behavior must be traced to the fact that the Hubbard interaction and the ionic potential compete locally on each site, while the Peierls modulation of the hopping amplitude tends to move electronic charge to the bonds between sites, thereby avoiding conflict with the Hubbard term. This difference is also reflected in the characteristic structures of the ionic and the Peierls terms in the bosonized versions of the Hamiltonian.

The important question remains about the nature of the insulating phase of the IHM for  $U > U_c$ . As we argued above the numerical search for the vanishing of the spin gap will remain ambiguous due to the necessity to rule out the possibility of a finite but exponentially small  $\Delta_S$ . To further analyze the BI and CI phases below and above  $U_c$ , we have calculated correlation functions in the ground state of the IHM using DMRG results for finite chains.

Fig. 6 shows the charge distribution  $\langle 0 | (n_{r,\uparrow} + n_{r,\downarrow} -$

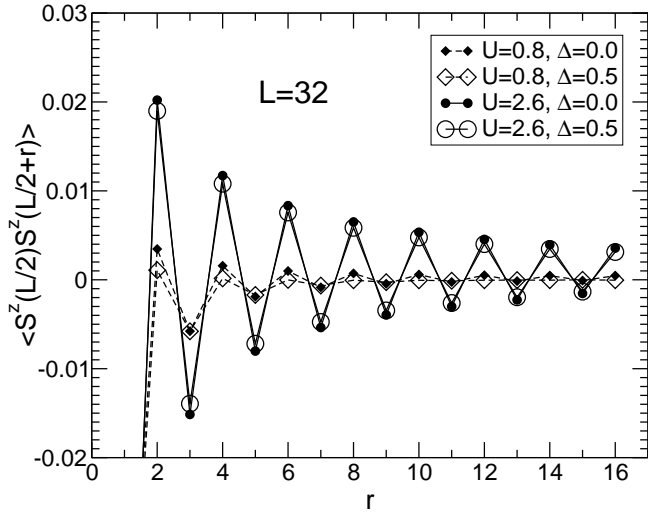


FIG. 7. Spin-spin correlation function in the ground state of the IHM for  $\Delta = 0.5t$  (open symbols) and the Hubbard model ( $\Delta = 0$ ) (full symbols) at  $U = 0.8t$  (diamonds) and  $U = 4t$  (circles). Chain length  $L = 32$ .

$1|0\rangle$  in the ground state of the Hubbard model and the IHM at  $U = 0.8t < U_c$  and  $U = 4t > U_c$  for a  $L = 32$  chain. The alternating pattern in the density distribution is well pronounced not only in the BI phase but also in the CI phase far beyond the critical point at  $U \gg U_c$ . For the  $L = 32$  chain the CDW is well established at distances  $l \sim L/2$  even at  $U = 4t$ . We note, that the attraction (or repulsion) of the charge from the chain edges, a well pronounced boundary effect in the BI phase, is absent at  $\Delta = 0$  and in the CI phase of the IHM. The amplitude of the CDW pattern smoothly decreases with increasing  $U$ . Our numerical data indicate that the alternating pattern in the electron density distribution in the IHM remains for arbitrary finite  $U$ .

Fig. 7 shows the DMRG results for the spin-spin correlation function  $\langle 0|S^z(L/2)S^z(L/2+r)|0\rangle$  in the ground state of the IHM at  $U = 0.8t < U_c$  and  $U = 4t > U_c$  in comparison with the spin correlators in the Hubbard model. In the BI phase at  $U = 0.8t$  the SDW correlations are almost completely suppressed on a scale of half the chain length. At  $U = 4t$  the amplitude of the SDW correlation in the CI phase of the IHM is slightly reduced in comparison to the Hubbard model at the same value of  $U$ . However, the large distance behavior of the spin correlations in the CI phase and the MI phase of the Hubbard model is similar. Therefore at arbitrary  $U > U_c$  the spin correlations in the CI phase of the IHM are almost identical to the Hubbard model. This equivalence, however, is valid up to the accuracy of an unresolvably small gap in the spin excitation spectrum.

To address the dimerization tendencies in the CI phase we have calculated the ground-state distribution of the normalized bond density

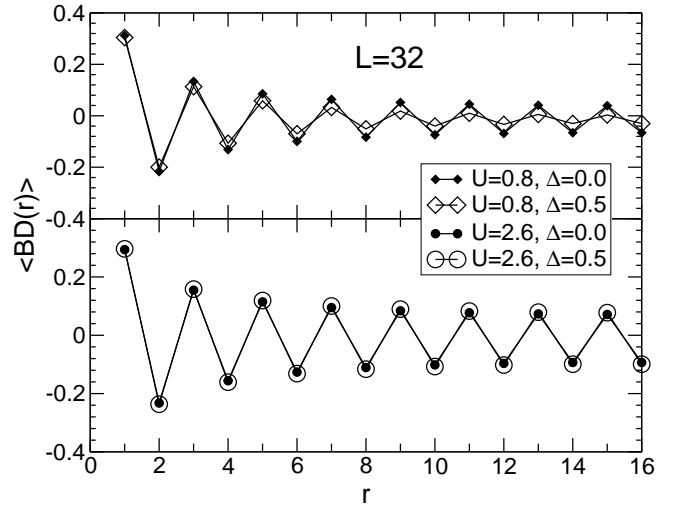


FIG. 8. Bond density correlation function in the ground state of the IHM for  $\Delta = 0.5t$  (open symbols) and the Hubbard model (full symbols) at  $U = 0.8t$  (diamonds) and  $U = 4t$  (circles).

$$BD(r) = \frac{\sum_{\sigma} \langle c_{r,\sigma}^{\dagger} c_{r+1,\sigma} + H.c. \rangle}{\frac{1}{L} \sum_{r,\sigma} \langle c_{r,\sigma}^{\dagger} c_{r+1,\sigma} + H.c. \rangle} - 1. \quad (47)$$

Fig. 8 shows the results of the DMRG calculations for a  $L = 32$  IHM chain and the Hubbard chain at  $U = 0.8t$  and  $U = 4t$ . The boundary effect of an open chain is strong and leads to a modulation of the bond density already for the pure Hubbard model. The comparison with the Hubbard chain indicates, that the ionic distortion leads to a weak suppression of the bond-density ordering at  $U < U_c$ , while at  $U > U_c$ , the amplitude of the bond-density modulations slightly increases in the CI phase.

To study the tendency in the IHM towards BOW ordering at the transition into the CI phase we compare the boundary induced alternating patterns of the bond density at  $\Delta = 0$  and  $\Delta = 0.5t$  as a function of  $U$ . For the open  $L = 32$  IHM chain the effect is clearly seen if we compare the corresponding bond densities in the central bond of the chain as shown in Fig. 9. In the BI phase at  $U < U_c$ , the ionic term reduces the bond density. However in the vicinity of the transition point and at  $U > U_c$  the bond density in the IHM is larger than in the pure Hubbard model. It is notable that this difference remains positive for arbitrary  $U > U_c$  and disappears only in the limit  $U \rightarrow \infty$ .

We conclude that the finite chain DMRG studies of the IHM indicate the presence of only one transition from the BI to the unconventional CI phase with long range CDW order for all  $U < \infty$ . In the CI phase the spin excitation spectrum is either gapless or characterized by an unresolvably small spin gap. If the spin gap is finite, we expect true long range BOW order coexisting with a CDW. If however the spin gap vanishes, SDW and the dimer-dimer correlations coexist in this phase with an identical decay at large distances in the presence of a

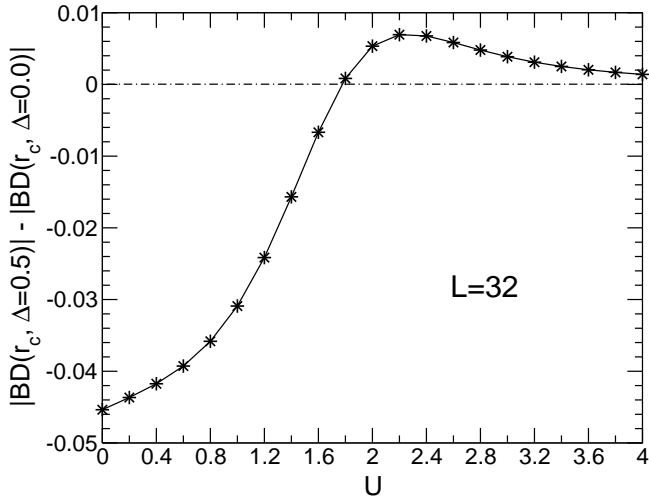


FIG. 9. Difference between the bond-charge density of the IHM with  $\Delta = 0.5t$  and the Hubbard model for  $\Delta = 0$  as a function  $U$ .  $r_c$  denotes the bond  $\langle r_c, r_c + 1 \rangle$  in the center of a  $L = 32$  chain.

finite CDW amplitude. The fact, however, that the spin gap is finite and equal to  $\Delta_C$  at the transition supports the scenario of a CI phase for  $U > U_c$  with a finite  $\Delta_S$  and coexisting long range CDW and BOW order.

## VII. OPTICAL CONDUCTIVITY

To further analyze the BI and CI phases we have calculated the frequency-dependent conductivity within the dynamical DMRG (DDMRG) approach, making use of the correction-vector technique described in Ref. [38]. Calculations were performed for  $L = 128$  sites with OBC using a Parzen filter to suppress the influence of the chain boundaries.

The real part of the dynamical conductivity  $\sigma(\omega)$  is determined from the linear response of the system to an external electromagnetic field. In the Kubo formalism,  $\sigma(\omega)$  is related to the imaginary part of the retarded current-current correlation function

$$\begin{aligned} \chi_{jj}(q, \omega) &= \frac{i}{La} \int_0^\infty d\tau e^{i\omega\tau} \langle \psi_0 | [j_{-q}(\tau), j_q(0)] | \psi_0 \rangle \\ &= \frac{\hbar}{La} \sum_{n \neq 0} \left( \frac{|\langle \psi_n | j_q | \psi_0 \rangle|^2}{\hbar\omega + (E_n - E_0) + i0^+} \right. \\ &\quad \left. - \frac{|\langle \psi_n | j_q | \psi_0 \rangle|^2}{\hbar\omega - (E_n - E_0) + i0^+} \right), \quad (48) \end{aligned}$$

with  $\tau$  the time index,  $a$  the distance between neighboring sites, and  $|\psi_n\rangle$  and  $E_n$  denoting the eigenstates and their respective energies. The paramagnetic current operator is defined by

$$j_q = -it \frac{ea}{\hbar} \sum_{l, \sigma} e^{iq l} \left( c_{l+1\sigma}^\dagger c_{l\sigma} - c_{l\sigma}^\dagger c_{l+1\sigma} \right), \quad (49)$$

where  $e$  is the electron charge. The structure of the current operator and the required matrix elements enforces the important selection rule that only transitions between states with different site-parity are allowed. The real part of the conductivity in the long-wavelength limit  $q = 0$  is given by

$$\sigma_1(\omega) = D\delta(\omega) + \sigma_1^{reg}(\omega > 0) \quad (50)$$

$$\sigma_1^{reg}(\omega > 0) = \frac{1}{\hbar\omega} \text{Im}\chi_{jj}(q = 0, \omega) \quad (51)$$

For the insulating phases of the IHM at half-filling the Drude weight either vanishes,  $D = 0$ , or is not defined for degenerate ground states, so that  $\sigma_1(\omega) = \sigma_1^{reg}(\omega)$ .

In the absence of interactions  $U = 0$ , the conductivity diverges as  $\sigma_1(\omega) \sim 1/\sqrt{\omega - \Delta_C}$  for  $\omega \rightarrow \Delta_C$  and  $\omega > \Delta_C$  [39]. We expect this behavior to persist upon increasing  $U$  over the entire BI phase. In order to test this expectation we have evaluated the optical conductivity in the BI phase by DDMRG [38]. For the correction-vector method a separate DMRG run has to be performed for each selected frequency  $\omega$ . In Fig. 10, the DDMRG results for a chain with  $L = 128$  sites and OBC are plotted for  $U = 3t$ . For the proper convergence of the correction-vector algorithm a finite broadening  $\eta = 0.1t$  was chosen in Eq. (48). For  $\Delta = 4t$ , the solid black line interpolating between the discrete data points at different frequencies was calculated by additionally applying the Lanczos vector method after the DMRG sweeps, obtaining the correlation function also in the vicinity of the selected frequencies [38]. One observes a dominant low-energy excitation peak above the optical gap at around  $E \approx 1.7t$ . The Lorentzian tail for  $E < 1.7t$  results from the necessarily large broadening. Also, in the correction-vector results the square-root divergence at the absorption edge is not visible due to the finite size of the system. However, it is to be anticipated from the dominant excitation peak above the gap edge.

For  $U > U_c$ , the situation is different, as demonstrated in Fig. 10, too, where we also show  $\sigma_1(\omega)$  for  $U = 3t$  and  $\Delta = 0.5t$ . The dashed line connecting the data points serves only as a guide to the eye. In the CI phase, the behavior of the optical excitations is expected to be similar to those of the repulsive Hubbard model, where  $\sigma_1(\omega) \sim \sqrt{\omega - \Delta_C}$  above the charge gap  $\Delta_C$  which in this case is identical to the optical gap [40]. In the inset of Fig. 10,  $\sigma_1(\omega)$  is plotted on a finer energy scale in the onset region above the gap edge. The solid black line is a fit to the DDMRG data obtained by convoluting  $\sqrt{\hbar\omega - \Delta_{opt}}$  with a Lorentzian of width  $\eta$ , i.e. by using the fit formula

$$\sigma_1(\omega) = \frac{A}{\hbar\omega\pi} \int_{\Delta_{opt}}^{\nu_{max}} d\nu \frac{\eta\sqrt{\nu - \Delta_{opt}}}{(\nu - \hbar\omega)^2 + \eta^2}, \quad (52)$$

where  $A$  is an adjustable prefactor and  $\nu_{max}$  the upper bound for the square-root dependence. The fit in Fig. 10 has been obtained using the parameter values  $A = 1.9t$ ,

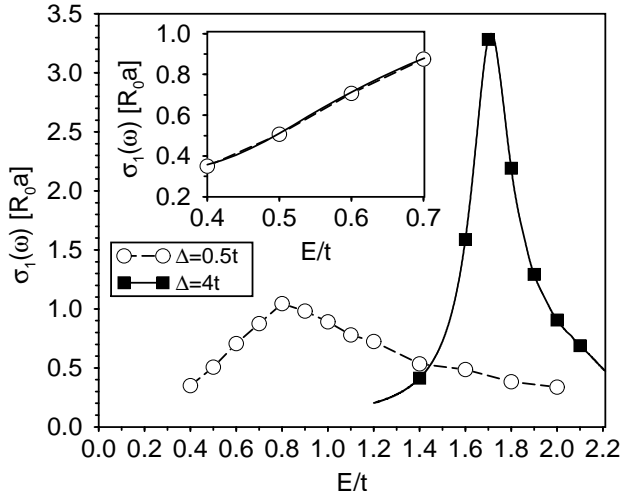


FIG. 10. Real part of the optical conductivity  $\sigma_1(\omega)$  in units of  $R_0 a = e^2 a / \hbar$  vs. energy  $E = \hbar \omega$  for the half-filled IHM for  $U = 3t$ . The results were obtained by DDMRG calculations using the correction-vector method for a chain with  $L = 128$  sites and OBC. A finite broadening  $\eta = 0.1t$  has been used. The selected  $\Delta$ -values correspond to the BI ( $\Delta = 4t$ ) and the CI ( $\Delta = 0.5t$ ) phase. The inset shows a fit (solid black line) to the onset region of  $\sigma_1(\omega)$  in the CI phase.

$\nu_{max} = 1.5t$ , and  $\Delta_{opt} = 0.48t$ . The value for  $\Delta_{opt}$  is close to the charge gap result presented in Fig. 4. A difference between  $\Delta_{opt}$  and  $\Delta_C$  can not be resolved within the accuracy of the DDMRG data. The agreement between the fit and the DDMRG results is quite striking. Thus, we conclude that the numerical results are in agreement with the behavior expected for a correlated (Mott) insulator in 1D. The qualitative behavior of  $\sigma_1(\omega)$  compares well with the results obtained for the Hubbard model at  $U = 3t$  [40].

Further consequences for the optical conductivity follow from the level crossing scenario discussed in the previous sections. On approaching  $U_c$  the ground and the first excited state become degenerate,  $E_1 \rightarrow E_0$ ; the matrix element  $\langle \psi_1 | j_{q=0} | \psi_0 \rangle$  between these states remains finite due to their different site parity eigenvalues. Therefore, the optical gap vanishes precisely at  $U_c$ . The critical point has been commonly referred to in the literature as “metallic”. However, by definition a metal is characterized not only by gapless excitations, but also by a finite Drude weight  $D > 0$ . Due to the ground-state degeneracy the Drude weight for  $U = U_c$  is not properly defined. Thus it follows that although the optical excitation gap vanishes in the IHM for  $U = U_c$ , it cannot be considered “metallic” in the usual sense. (Following the definition of W. Kohn a metal has a finite Drude weight,  $D > 0$  [41].)

We emphasize that the optical conductivity was so far evaluated in the BI and the CI phase sufficiently far from the critical point. Our currently achievable accuracy does

not allow safe conclusions for the optical conductivity in the critical region around  $U_c$ . At  $U_c$  the charge gap  $\Delta_C$  remains finite while the optical gap vanishes. This special situation demands that near below  $U_c$  the optical conductivity has an isolated peak below the onset of the continuum for optical absorption. The energy of the isolated peak corresponds to the energy difference of the individual ground states in each site-parity sector with  $P = \pm 1$ . Resolving this remarkable feature will remain a challenge for future numerical simulations.

## VIII. CONCLUSIONS

Our combined analytical and numerical analysis clarifies the ground-state structure of the IHM. A single transition at a critical  $U_c(\Delta)$  separates a CDW-BI from a CI phase with finite charge and optical excitation gaps and most likely also a finite spin excitation gap. Above  $U_c$ , CDW and BOW order coexist and persist for all  $U > U_c$ . No secondary transition into a true MI phase occurs which - in fact - would have a higher symmetry than the IHM itself. The insulator-insulator transition on finite chains of the IHM results from a ground-state level crossing of the site-parity sectors with  $P = \pm 1$ . The BI phase has a unique ground state with  $P = +1$  while the ground state in the CDW + BOW phase above  $U_c$  is necessarily two-fold degenerate. The critical point  $U_c(\Delta)$  is characterized by the remarkable situation that the optical absorption gap vanishes while the spin and charge excitation gaps remain finite and equal. The distinction between the optical and the charge gap is the key feature for the structure of the insulating phases of the IHM. Refined numerical studies of the optical conductivity in the critical region define therefore the future task.

The existence of an insulator-insulator transition in the IHM at half-filling naturally raises the question of whether a ground state phase transition finds its continuation also when the system is doped away from half-filling. The possible consequences for the dynamics of doped charge carriers and for the phenomenon of spin-charge separation will be the topic of future investigations in the IHM.

## ACKNOWLEDGMENTS

We thank D. Baeriswyl, M. Fabrizio, A. Nersisyan, B. Normand, H. Fehske, and T. Vekua for helpful discussions and R. Noack for instructive comments on the DMRG method. This work was supported by the Deutsche Forschungsgemeinschaft (DFG) through SP 1073. APK also acknowledges support through Sonderforschungsbereich 484 of the DFG. GIJ and MS acknowledge support by the SCOPES grant N 7GEPJ62379.

- [1] For a review see: M. Imada, A. Fujimori, and Y. Tokura, *Rev. Mod. Phys.* **70**, 1039 (1998).
- [2] D. H. Lee and R. Shankar, *Phys. Rev. Lett.* **65**, 1490 (1990).
- [3] C. Aebischer, D. Baeriswyl, and R. M. Noack, *Phys. Rev. Lett.* **86**, 468 (2001).
- [4] J. Sólyom, *Adv. Phys.* **28**, 201 (1979); *J. Voit, Rep. Prog. Phys.* **57**, 977 (1995).
- [5] M. Nakamura, *J. Phys. Soc. Jpn.* **68**, 3123 (1999); *Phys. Rev. B* **61**, 16377 (2000).
- [6] P. Sengupta, A.W. Sandvik, and D.K. Campbell, *Phys. Rev. B* **65**, 155113 (2002).
- [7] N. Nagaosa and J. Takimoto, *J. Phys. Soc. Jpn.* **55**, 2735 (1986); N. Nagaosa, *ibid.* **55**, 2754 (1986).
- [8] M. Fabrizio, A. O. Gogolin, and A. A. Nersesyan, *Phys. Rev. Lett.* **83**, 2014 (1999); *Nucl. Phys. B* **580**, 647 (2000).
- [9] N. Gidopoulos, S. Sorella, and E. Tosatti, *Eur. Phys. J. B* **14**, 217 (2000).
- [10] R. Resta and S. Sorella, *Phys. Rev. Lett.* **74**, 4738 (1995).
- [11] T. Wilkens and R. M. Martin, *Phys. Rev. B* **63**, 235108 (2001).
- [12] Y. Anusooya-Pati, Z. G. Soos, and A. Painelli, *Phys. Rev. B* **63**, 205118 (2001).
- [13] M.E. Torio, A.A. Aligia, and H.A. Ceccatto, *Phys. Rev. B* **64**, 121105 (2001).
- [14] J. B. Torrance *et al.*, *Phys. Rev. Lett.* **46**, 253 (1981); *ibid.* **47**, 1747 (1981).
- [15] T. Mitani *et al.*, *Phys. Rev. Lett.* **53**, 842 (1984); Y. Tokura *et al.*, *Sol. State Comm.* **43**, 757 (1982); *Mol. Cryst. Liq. Cryst.* **125**, 71 (1985); T. Mitani *et al.*, *Phys. Rev. B* **35**, 427 (1987); K. Takaoka *et al.*, *ibid.* **36**, 3884 (1987); Y. Tokura *et al.*, *ibid.* **38**, 2215 (1988).
- [16] A. Girlando, F. Marzola, C. Pecile, and J.B. Torrance, *J. Chem. Phys.* **79**, 1075 (1983).
- [17] M. LeCointe *et al.*, *Phys. Rev. B* **51**, 3374 (1995).
- [18] B. Horovitz and J. Sólyom, *Phys. Rev. B* **35**, 7081 (1987).
- [19] A. Girlando and A. Painelli, *Phys. Rev. B* **34**, 2131 (1986).
- [20] A. Painelli and A. Girlando, *Phys. Rev. B* **37**, 5748 (1988).
- [21] T. Egami, S. Ishihara, and M. Tachiki, *Science* **261**, 1307 (1993).
- [22] S. Ishihara, T. Egami, and M. Tachiki, *Phys. Rev. B* **49**, 8944 (1994).
- [23] L. T. Hudson, *Phys. Rev. B* **47**, 1174 (1993).
- [24] T. Neumann *et al.*, *Phys. Rev. B* **46**, 10623 (1992).
- [25] H.M. McConnell *et al.*, *Annu. Rev. Phys. Chem.* **17**, 237 (1966).
- [26] G. Ortiz, P. Ordejón, R. M. Martin, and G. Chiappe, *Phys. Rev. B* **54**, 13515 (1996).
- [27] Y. Takada and M. Kido, *J. Phys. Soc. Jpn.* **70**, 21 (2001).
- [28] S. Qin, J. Lou, T. Xiang, G. Tian, and Z. Su, preprint cond-mat/0004162, unpublished.
- [29] A. H. MacDonald, S. M. Girvin, and D. Yoshioka, *Phys. Rev. B* **37**, 9753 (1988).
- [30] M. Takahashi, *J. Phys. C* **10**, 1289 (1977).
- [31] F. D. M. Haldane, *Phys. Rev. B* **25**, 4925 (1982); K. Okamoto and K. Nomura, *Phys. Lett. A* **169**, 433 (1993); G. Castilla, S. Chakravarty, and V. J. Emery, *Phys. Rev. Lett.* **75**, 1823 (1995).
- [32] For a review see A. O. Gogolin, A. A. Nersesyan, and A. M. Tsvelik, *Bosonization and strongly correlated systems*, Cambridge University Press (1998).
- [33] C. Lanczos, *J. Res. Natl. Bur. Stand.* **45**, 255 (1950).
- [34] S. R. White, *Phys. Rev. Lett.* **69**, 2863 (1992); *Phys. Rev. B* **48**, 10345 (1993).
- [35] I. Peschel, X. Wang, M. Kaulke, K. Hallberg (Eds.): *Density-Matrix Renormalization*, Springer (1999).
- [36] R. Noack, private communication.
- [37] K. A. Hallberg, *Phys. Rev. B* **52**, R9827 (1995).
- [38] T. D. Kühner and S. R. White, *Phys. Rev. B* **60**, 335 (1999).
- [39] F. Gebhard, K. Bott, M. Scheidler, P. Thomas, and S. W. Koch, *Phil. Mag. B* **75**, 1 (1997).
- [40] E. Jeckelmann, F. Gebhard, and F. H. L. Essler, *Phys. Rev. Lett.* **85**, 3910 (2000).
- [41] W. Kohn, *Phys. Rev.* **133**, A171 (1964).